Exp. Theo. NANOTECHNOLOGY 10 (2026) 1601-1609 https://doi.org/10.56053/10.3.1601

Comparative study on photocatalytic degradation of methylene blue using $CoFe_2O_4$, $NiFe_2O_4$ and $CoNiFe_2O_4$ prepared by sol-gel method

Zainab R. Muslim[1,], Ban M.Alshabader[1], Asmaa.S.Khalil[1], Zina A. Al Shadidi[2], Raied K. Jamal[1], Ahmed M .Hammed[1], Ali Q. Kadhum[1]*

[1]University of Baghdad, College of Science, Physics Department, Baghdad, Iraq
[2]Department of Radiology, Al Maoon University College, Baghdad, Iraq
[*]) Email: Zainab.muslim@sc.uobaghdad.edu.iq

Received 27/4/2026, *Received in revised form* 23/5/2026, *Accepted* 19/6/2026, *Published* 15/7/2026

This work focuses on synthesizing ferrites specifically cobalt ($CoFe_2O_4$), nickel ferrite ($NiFe_2O_4$), and mixed ferrites cobalt nickel ferrite ($CoNiFe_2O_4$), via the sol gel method for use in photocatalytic degradation of methylene blue (MB) in water treatment applications. Using a glass substrate and pulsed laser deposition, nanostructured thin films are created. Utilizing X-ray diffraction, the structural properties of these ferrites are investigated. The findings showed that the ferrites formed in a crystalline cubic shape. According to atomic force microscope utilization chart ,the granularity cumulating distribution, the average diameter for $NiFe_2O_4$, $CoFe_2O_4$, and $CoNiFe_2O_4$ are 83.8, 86.7, and 83.4 nm, respectively, according to atomic force microscopy. It has been demonstrated in field emission microscopic images that ferrite nanoparticles agglomerate because of their magnetic properties and the binding of parent particles held by surface interaction, like the Van Der Waals force, between them. The energy gap for nano-ferrites is examined to explain the photocatalytic activity of methylene blue dye. The $CoFe_2O_4$ has the smallest energy gap (Eg=1.97 eV). This is due of improved charge separation, less recombination, and improved surface characteristics brought about by nickel incorporation, $NiFe_2O_4$ shows superior catalyst efficiency even though $CoFe_2O_4$ has a lower band gap. This increases the photocatalytic degradation efficiency of $CoNiFe_2O_4$.

Keywords: Comparative; Energy gap; Photocatalytic; Methylene blue; Characterization.

1. INTRODUCTION

Ferrites in nanotechnology have been widely known as excellent photocatalysts thanks to their outstanding properties such as relatively narrow band gaps, chemical, and thermal stability, excellent magnetic properties, and low cost. They have recently been explored for their visible-light activity for various photocatalysis applications. Prakash, J et al. [1] prepared a series of nickel-modified cobalt ferrite nanocatalysts with the composition $Co1\text{-}xNixFe_2O_4$ (x=0.1–0.5) through sol-gel auto-combustion route to investigate their electro/photocatalytic. With Ni doping, there is an increase in the band gap from 1.75 to 2.11 eV. Metal oxides and ferrites play a crucial role in various advanced applications, particularly in energy storage and water purification. In batteries and supercapacitors, metal oxides and transition metal oxides are widely used due to their high charge storage capacity, fast electron transfer and enhancing the efficiency of electrical devices [2]. On the other hand, nanocomposites are used to create materials with enhanced interlaminar toughness [3] and for ferrite compounds like $NiFe_2O_4$ and $CoFe_2O_4$ they exhibit unique magnetic and electrical properties, making them effective in water purification and as electrode materials that improve electrochemical performance and thermal stability [4-6]. The metal ions' size and charge, which counterbalance the oxygen ions' charge, as well as their relative numbers, determine the structural symmetries of garnets, hexagons, and cubic [4]. The preparation method, sintering condition, and quantity of constituent metal oxides all have a significant impact on the number of dopants or substituted elements as well as constituent metal oxides. It is found that the composition and microstructure of ferrites, which are impacted by processing conditions, significantly affect their magnetic and structural characteristics. With the structural formula MFe_2O_4 (where M=divalent metal ion, such as Mg, Zn, Ni, Co, Cu, etc.), One kind of soft magnetic material is spinel ferrite particles at the nano-scale. Because of their significant properties, such as their lower melting point, low magnetic transition temperature, large expansion coefficient, and high specific heat. Because of their properties, spinel ferrites are utilized in transformer cores, antenna rods, memory chips, permanent magnets, high-density magnetic recording media, photoelectric devices [4], catalysis [5], sensors [6], micro-wave devices [7], and magnetic pigments [8]. Ferrites' electrical and magnetic characteristics are crucial, and they are influenced by a number of factors, including manufacturing conditions, sintering temperature and duration, chemical makeup, and the type and quantity of additives used [9]. The aim of the research is to investigate the effect of mixing ferrites on the photocatalytic activity using MB dye. The objective of this work is to show the effect of the degradation of Methylene Blue (MB) in water treatment applications. Powder of $CoFe_2O_4$, $NiFe_2O_4$, and $CoNiFe_2O_4$ are prepared for use as photocatalysts for water treatment applications.

2. EXPERIMENTAL

2.1. Preparation of ferrites

- Mixing of Materials: Combining distilled water (20 ml) with nickel and iron precursors, assuming the standard sol gel for $NiFe_2O_4$ requiring a Ni:Fe ratio of 1:2 and metal: citric acid ratio of 1:1 ratio.
- Gel Formation: The mixture is heated to 80 °C for 1 h with continuous stirring until the water evaporates and a gel form.
- Drying: The gel is dried in an oven at 150 °C for 4 h.
- Calcination: The dried powder is calcined at 700 °C for 2 h to obtain a pure crystalline form.
- PLD Film Formation: The final crystalline powder press as pellet with diameter (1-2 inch) and thickness of 4 mm is used to create thin films in the PLD vacuum chamber at 2.5×10-2 Torr with a Nd:YAG laser.

2.2. Methylene Blue (MB) solution preparation

A weight of 0.5 mg of MB powder is dissolved in 100 ml of distilled water to create 5 ppm of MB dye solutions. At room temperature, 20 ml of 5 ppm MB dye solutions are mixed with 0.01 g of ferrites. To establish a uniform composition, solutions are put on a magnetic stirrer. Each solution is then subjected to UV light for varying lengths until the reaction is stopped. The beaker and the UV source are separated by 30 cm. UV-visible spectroscopy is employed to examine the solution's change in absorbance.

3. RESULTS AND DISCUSSION

3.1. X-ray diffraction for nickel ferrite, cobalt ferrite, and cobalt nickel ferrite.

The XRD spectra of $NiFe_2O_4$, $CoFe_2O_4$. and $CoNiFe_2O_4$ are displayed in Fig. 1. The spectra of $NiFe_2O_4$ demonstrate the formation of a cubic structure (JCPDS NO. 98-020-1149).

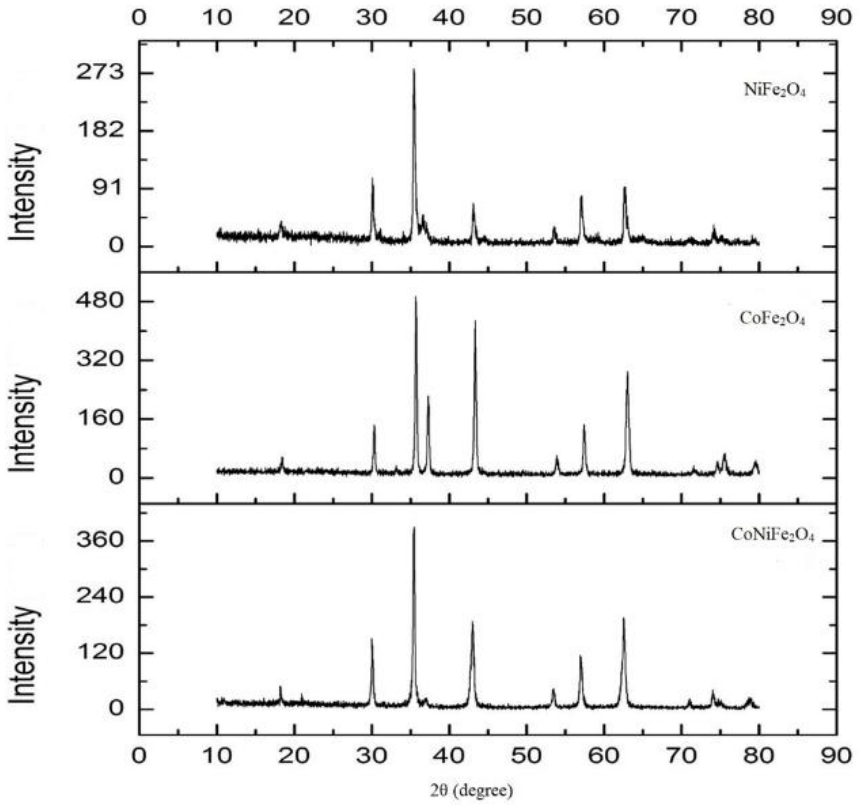

Figure 1 XRD spectra of ferrites ($NiFe_2O_4$) ;($CoFe_2O_4$); and ($CoNiFe_2O_4$).

The construction of a cubic structure is indicated by the primary peaks at 18.4°, 30.3°, 35.7°, 37.3°, 43.4°, 53.8°, 57.3°, 62.99°, 71.5°, 74.5°, and 79.6° that correspond to planes (111), (220), (311), (222), (400), (422), (511), (440), (620), (533), and (444) respectively. The $NiFe_2O_4$ is consistent with the findings of [10]. The spectra of $CoFe_2O_4$, gettings the formation of a (cubic structure) (JCPDS NO. 98-010-9044) [11]. The development of the cubic structure $CoFe_2O_4$ is indicated by the principal peaks at

18.3°, 30.1°, 35.4°, 37.1°, 43.1°, 53.4°, 56.96°, 62.5°, 70.96°, and 73.99°, with plans (111), (220), (311), (222), (400), (422), (511), (440), (620), indicates the formation of cubic structure $CoFe_2O_4$ this agrees with that shown by other researchers [11]. The spectra of mixed cobalt and $CoNiFe_2O_4$, demonstrate the formation of a cubic structure (JCPDS NO. 98-016-6741) [12]. It is indicated by the prominent peaks at 18.3°, 30.1°, 35.5°, 37.1°, 43.1°, 53.5°, 57°, 62.6°, and 75.1° have plans (111), (220), (311), (222), (400), (422), (511), (440), and (620) respectively. This is in agreement with the conclusion reported by [13].

3.2. Field emission scanning electron microscopy images of thin films

The surface morphology is investigated using field emission scanning electron microscopy (FE-SEM), as shown in Figure 1.

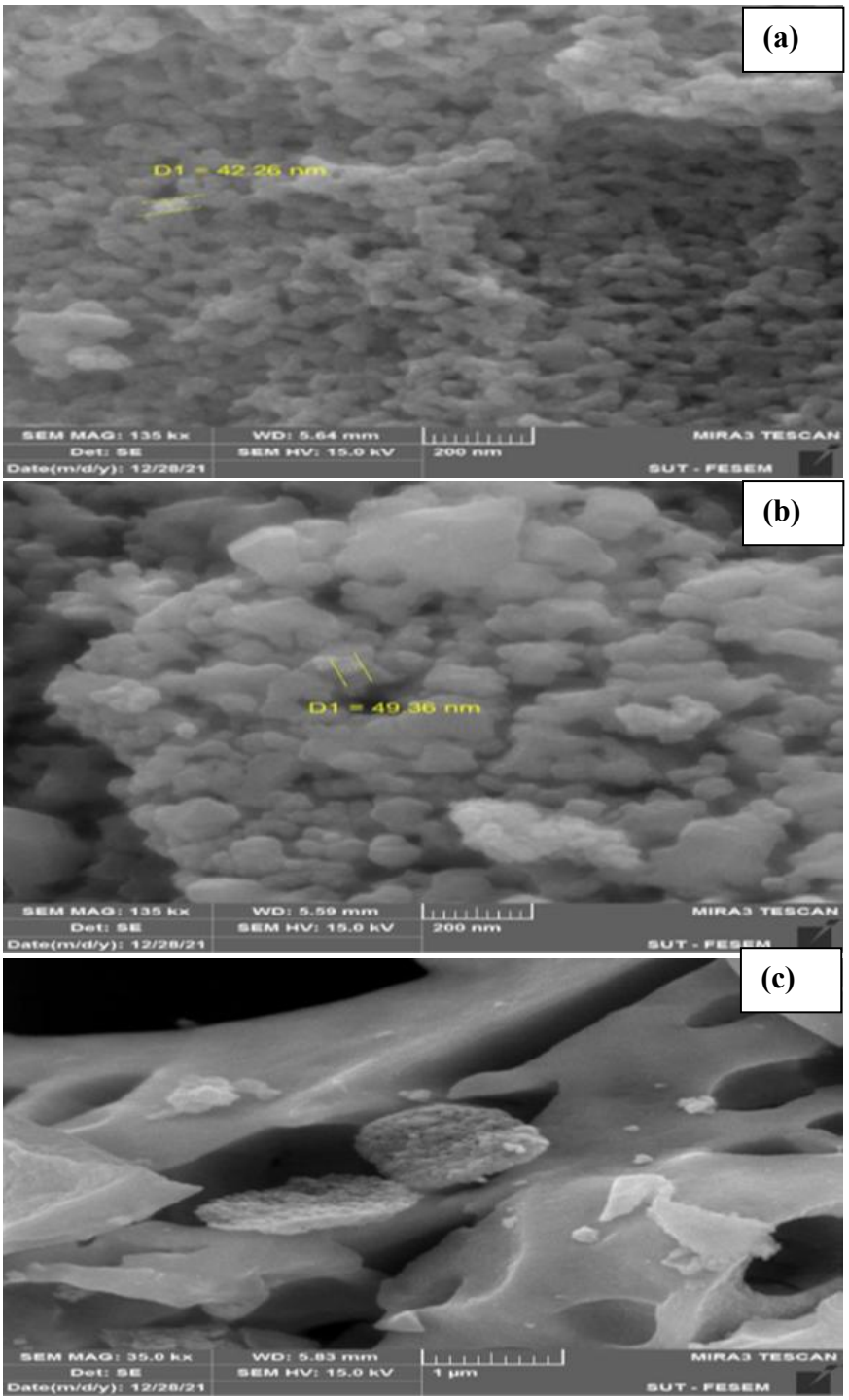

Figure 1 FESEM images for (a) $NiFe_2O_4$, (b) $CoFe_2O_4$, (c) mixed $NiFe_2O_4$,and $CoFe_2O_4$.

The morphological investigation of all material surfaces using SEM analysis revealed spherical distribution with a high degree of agglomeration and various surface morphologies. The morphological features of $NiFe_2O_4$ show that the particles are agglomerated and homogenous due to their magnetic interaction. The particle size of $CoFe_2O_4$ is often more significant than that of $NiFe_2O_4$, but $CoNiFe_2O_4$

is in the middle of the $NiFeO_4$ and $CoFe_2O_4$ particle size (A) balance between Co^{2+} and Ni^{2+} affects nucleation and growth i.e. mixed cation distribution modifies structural and magnetic properties.

3.3. Atomic force microscopic results

Figure 3, displays atomic force microscopy micrographs of $NiFe_2O_4$, $CoFe_2O_4$, and $CoNiFe_2O_4$. samples. The samples exhibit uniform distribution of nanostructures and appear to have a uniform grain distribution across their surface. Table 1, lists the average grain size, which represents the dimensions of the nanostructure for these samples. The AFM images themselves visually confirm the Surface topography, showing the distinct nanostructure morphology for each of ferrites.

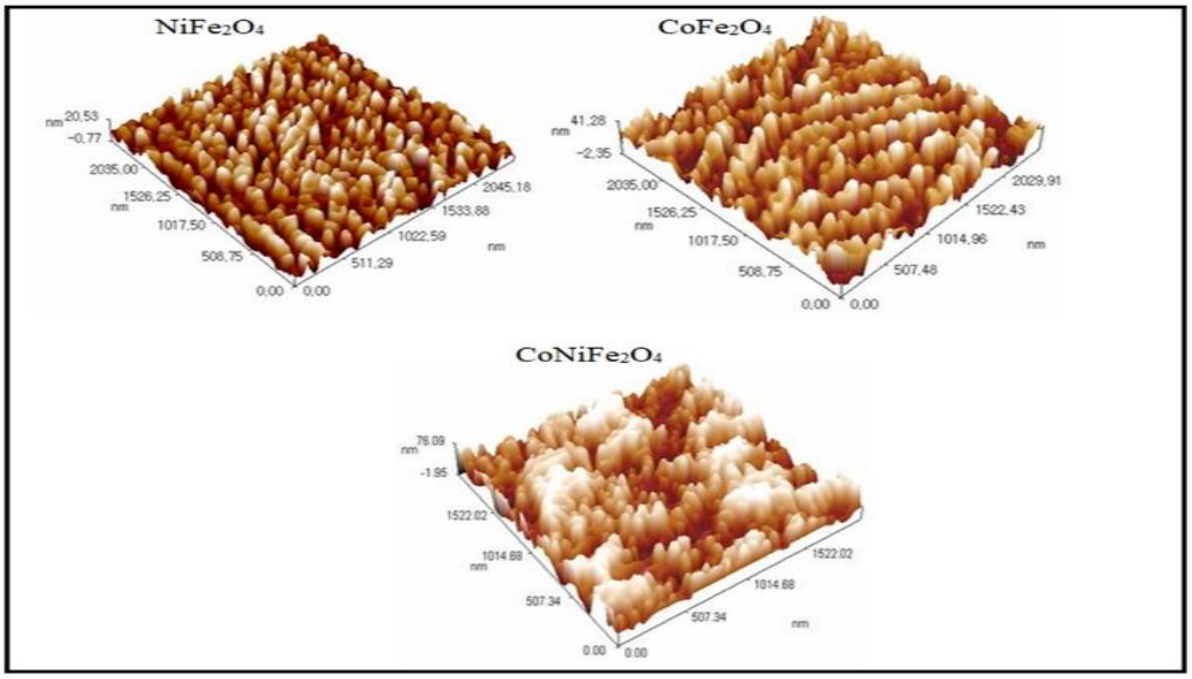

Figure 3 2D AFM micrograph, micrograph for $NiFe_2O_4$ $CoFe_2O_4$, and $CoNiFe_2O_4$.

Table 1 The average grain size and average roughness of the AFM samples.

Samples	Grain Size (nm)	Roughness (nm)
$NiFe_2O_4$	83.8	4.24
$CoFe_2O_4$	86.7	7.64
$CoNiFe_2O_4$	83.4	16.9

3.4. Energy gap and photocatalytic degradation

Figures 4(a), (b), (c), and (d) illustrate the UV-visible absorbance spectrum of methylene blue (MB) in distilled water, alongside the photocatalytic activity demonstrated by the ferrite materials. The MB dye, characterized by an absorbance peak at 663 nm, is successfully degraded photocatalytically by the samples under UV-visible light irradiation. Further investigation, utilizing MB as a representative

organic pollutant, focused on the photocatalytic efficacy of both pure and mixed ferrites. Notably, $CoFe_2O_4$ showed higher efficiency for MB dye degradation when compared to $NiFe_2O_4$.

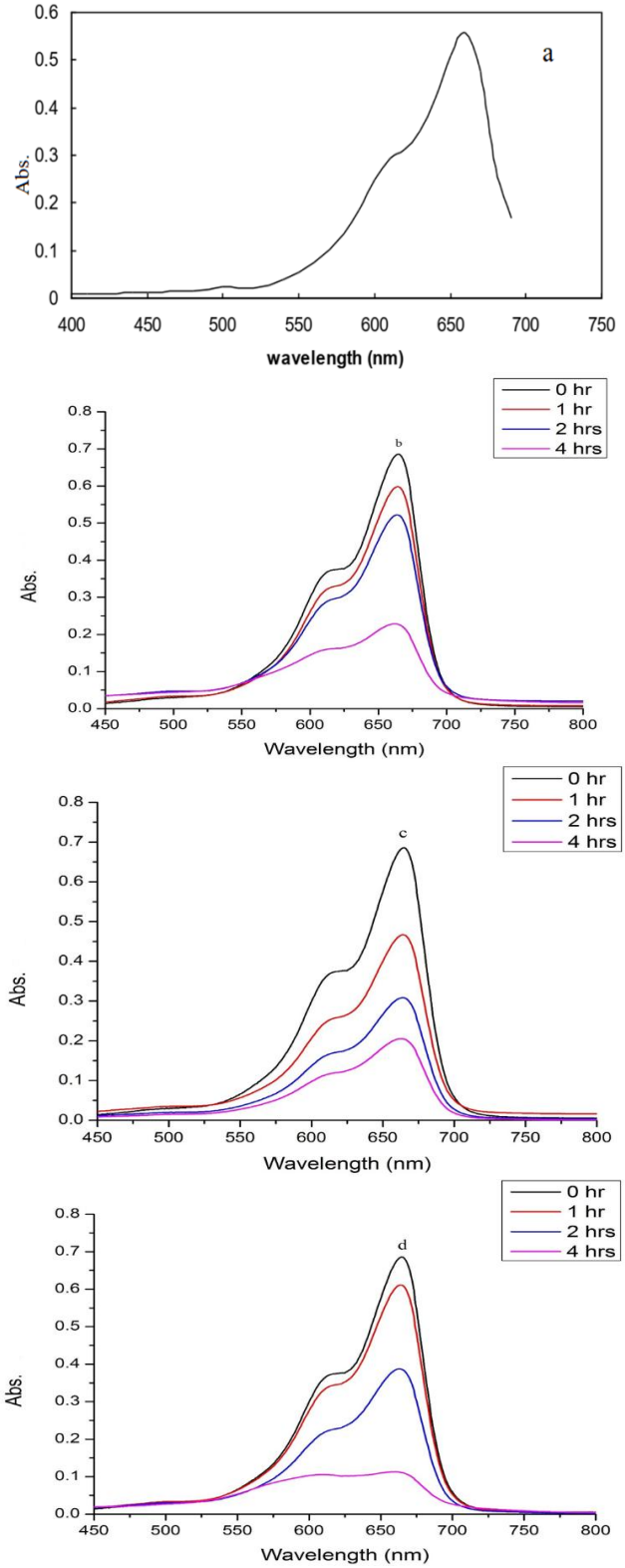

Figure 4 UV-visible absorbance spectra of (a) MB in distilled water, and photocatalytic activity for (b) $NiFe_2O_4$, (c) $CoFe_2O_4$ and(d) $CoNiFe_2O_4$ materials ferrite.

The linear trend in the spectrum dependence of $(\alpha h\upsilon)^2$ across a restricted range of photon energies ($h\upsilon$), as shown in Figure 5 to compute the energy band gap related to ferrites, as seen in Table 2. Figure 5 make it clear that all samples show absorption edges for $CoFe_2O_4$, $NiFe_2O_4$, and $CoNiFe_2O_4$.The linear trend in the spectrum dependence of $(\alpha h\upsilon)^2$ across a restricted range of photon energies ($h\upsilon$) is used to compute the energy band gap related to ferrites [10-13]. The sample with the smallest energy gap 1.97 eV is $CoFe_2O_4$. Since the Ni^{2+} (3d8) ion is smaller than the Co ion (3d7), deeper Ni^{2+} states are produced via stronger electrostatic contact, which is most likely the cause of the band gap tendency [14-16]. When switching from $CoFe_2O_4$ to $NiFe_2O_4$, the energy difference between the occupied and unoccupied levels increases, assuming all other factors remain constant [17–20].

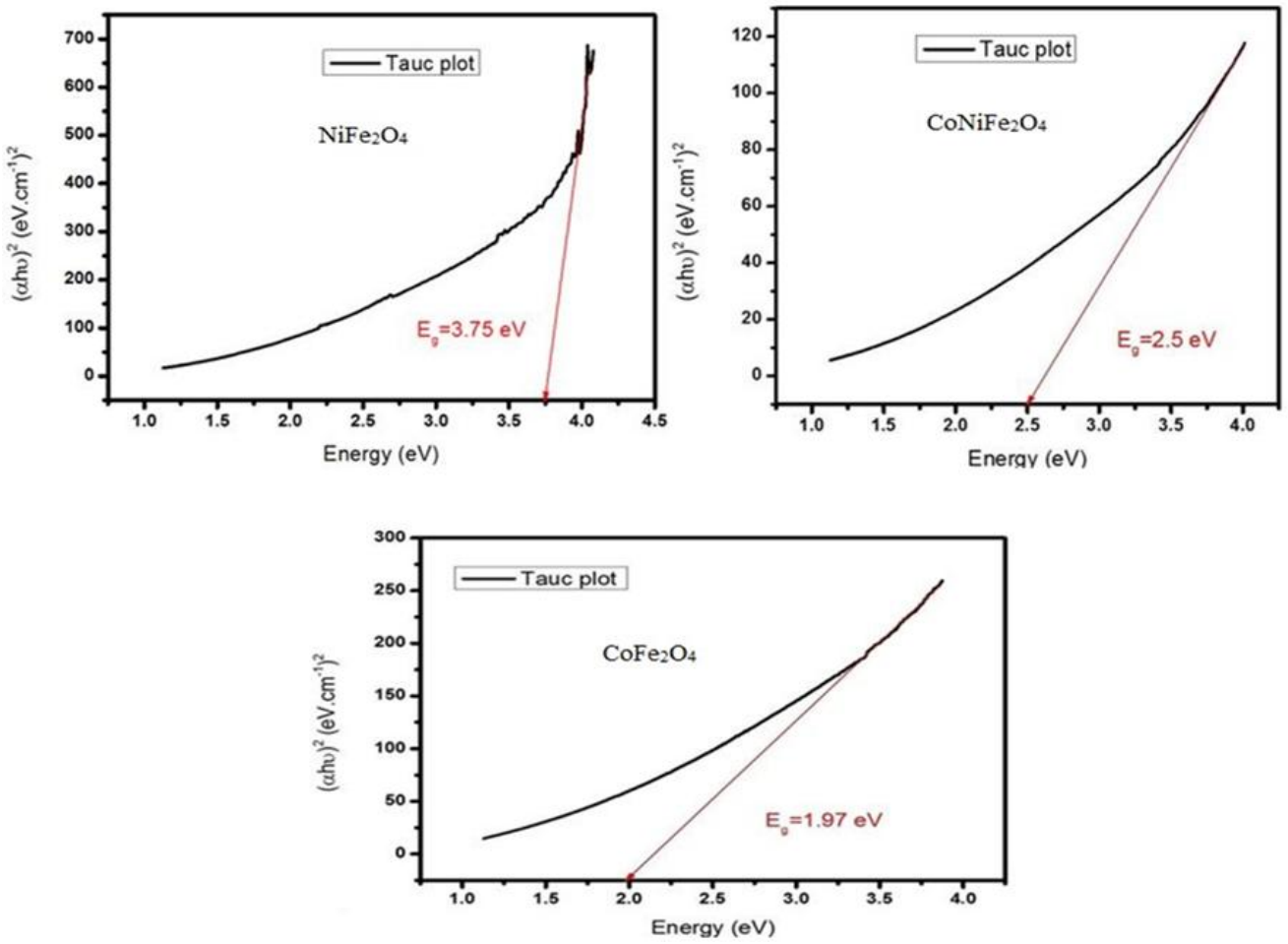

Figure 5 $(\alpha h\upsilon)^2$ vs. Energy gap of $NiFe_2O_4$, $CoNiFe_2O_4$ and $CoFe_2O_4$.

Table 2 The energy gap of the ferrites.

Samples	Energy gap (eV)
$NiFe_2O_4$	3.75
$CoFe_2O_4$	1.97
$CoNiFe_2O_4$	2.5

The factors influencing photocatalytic activity, focus on the size and surface properties of photocatalyst particles. The oxidation state of ferrites and hydroxyl radical concentration significantly impact their efficiency [21-23]. When exposed to UV light, ferrites generate electron-hole pairs, which react with water and hydroxyl ions, producing reactive species like superoxide anions and hydroxyl radicals [24, 25]. These species break down various substances, including synthetic dyes. Adding $NiFe_2O_4$ to $CoFe_2O_4$ enhances efficiency compared to their individual effects. This improvement is linked to increased absorption and hydroxyl radical generation, which accelerate pollutant degradation [14]. Optimizing photocatalyst size and light exposure can enhance their ability to degrade contaminants, making them useful for environmental applications [26]. Photocatalytic activity depends on the material's ability to generate electron-hole pairs when exposed to light. Superoxide anions and hydroxyl radicals, produced through these reactions, help break down pollutants [27-30]. The efficiency of ferrites can be improved by combining different metal ferrites, such as $NiFe_2O_4$ and $CoFe_2O_4$, which enhances light absorption and radical production. Modifying ferrite composition and light exposure can optimize photocatalysis for environmental applications. The effect of adding $NiFe_2O_4$ to $CoFe_2O_4$ on photocatalytic activity [31-33]. It states that this addition leads to higher dye absorption after 4 h, increasing the generation of hydroxyl radicals (•OH), which help break down organic pollutants and enhance the rate of photodegradation [15-20]. This effect is attributed to the preference of Ni^{+2} ions for octahedral sites in the crystal lattice, which enhances the photocatalytic activity of mixed ferrites compared to their individual properties. Additionally, in nano-sized nickel ferrites; a lower energy gap significantly increases the production of hydroxyl radicals, thereby improving the photocatalytic activity of $CoNiFe_2O_4$ [21 - 22].

4. CONCLUSIONS

Mixed ferrite proves to be an effective photocatalyst, demonstrating that the combination in the ferrite structure optimizes the material's properties for the degradation of organic pollutants like Methylene Blue in water treatment applications.

References

[1] M. Enneffati, M. Rasheed, B. Louati, K. Guidara, R. Barillé, Optical and Quantum Electronics, 51 (2019) 1. https://doi.org/10.1007/s11082-019-2015-5
[2] R. Fouad, Z. Raheem, Journal of Physics: Conference Series, 1879 (2021) 032066. https://doi.org/10.1088/1742-6596/1591/1/012003
[3] A. Kadhum, Z. R. Muslim, H. I. Jaffer, Acta Physica Polonica A, 135 (2019) 1126. https://doi.org/10.12693/APhysPolA.135.1126
[4] Z. A. Al Shadidi, M. H. Suhail, A. K. Falih, Z. R. Muslim, F. A. H. Mutlak, Journal of Optics (2025) 111198. https://doi.org/10.1007/s12596-025-02660-4
[5] M. L. Aparna, A. N. Grace, P. Sathyanarayanan, N. K. Sahu, Journal of Alloys and Compounds, 745 (2018) 385. https://doi.org/10.1016/j.jallcom.2018.02.127
[6] Haitham Mohammed Ibrahim Al-Zuhairi, Iqbal alshalal, Hind H. Abbood, M. Al Nuaimi, Experimental and Theoretical NANOTECHNOLOGY, 10 (2026) 855 https://doi.org/10.56053/10.S.855
[7] Z. R. Muslim, A. Q. Kadhum, Journal of Physics: Conference Series, 1591 (2020) 012005. https://doi.org/10.1088/1742-6596/1591/1/012005
[8] A. J. Hussein, M. N. Al-Darraji, M. Rasheed, M. A. Sarhan, IOP Conference Series: Earth and Environmental Science, 1262 (2023) 022005. https://doi.org/10.1088/1755-1315/1262/2/022005

[9] S. Baruah, M. Najam Khan, J. Dutta, Environmental Chemistry Letters, 14 (2016) 1. https://doi.org/10.1007/s10311-015-0542-2
[10] A. Q. Kadhum, Z. R. Muslim, Z. A. Al Shadidi, Experimental and Theoretical NANOTECHNOLOGY, 9 (2025) 87. https://doi.org/10.56053/9.S.87
[11] Z. R. Muslim, A. Q. Kadhum, Z. A. Al Shadidi, Experimental and Theoretical NANOTECHNOLOGY, 9 (2025) 79. https://doi.org/10.56053/9.S.79
[12] A. M. Hammed, Z. R. Muslim, IOP Conference Series: Materials Science and Engineering, 928 (2020) 072019. https://doi.org/10.1088/1757-899X/928/7/072019
[13] M. Enneffati, B. Louati, K. Guidara, M. Rasheed, R. Barillé, Journal of Materials Science: Materials in Electronics, 29 (2018) 171. https://doi.org/10.1007/s10854-017-7901-7
[14] A. Zubaidi, L. M. Asaad, I. Alshalal, M. Rasheed, Journal of the Mechanical Behavior of Materials, 32 (2023) 1. https://doi.org/10.1515/jmbm-2022-0302
[15] A. A. Abdulrahman, M. Rasheed, S. Shihab, Journal of Physics: Conference Series, 1879 (2021) 022118. https://doi.org/10.1088/1742-6596/1879/2/022118
[16] T. M. Noori, I. Hussein, N. A. Ali, A. R. Polu, Z. R. Muslim, M. K. Jawad, A. A. Kareem, H. K. Ismail, Fullerenes, Nanotubes and Carbon Nanostructures (2025). https://doi.org/10.1080/1536383X.2025.2520572
[17] A. Jaber, M. Ismael, T. Rashid, M. A. Sarhan, M. Rasheed, I. M. Sala, Eureka: Physics and Engineering, 4 (2023) 29. https://doi.org/10.21303/2461-4262.2023.002770
[18] R. F. Kadhum, Z. R. Muslim, Journal of Physics: Conference Series, 1591 (2020) 012003. https://doi.org/10.1088/1742-6596/1591/1/012003
[19] S. Hussein, N. A. Ali, A. Shawqi Khalil, Z. R. Muslim, M. K. Jawad, AIP Conference Proceedings, 3229 (2024) 070017. https://doi.org/10.1063/5.0236824
[20] E. Kadri, et al., Journal of Alloys and Compounds, 705 (2017) 708. https://doi.org/10.1016/j.jallcom.2017.02.117
[21] M. Hjiri, N. H. Alonizan, M. M. Althubayti, Journal of Materials Science: Materials in Electronics, 30 (2019) 15379. https://doi.org/10.1007/s10854-019-01914-9
[22] O. Alabdali, A. Guessab, Filomat, 34 (2020) 601. https://doi.org/10.2298/FIL2002601A
[23] H. M. I. Al-Zuhairi, I. Alshalal, H. H. Abbood, M. Al Nuaimi, Experimental and Theoretical NANOTECHNOLOGY, 10 (2026) 855. https://doi.org/10.56053/10.S.855
[24] H. M. I. Al-Zuhairi, I. Alshalal, H. H. Abbood, M. Al Nuaimi, Experimental and Theoretical NANOTECHNOLOGY, 10 (2026) 1093. https://doi.org/10.56053/10.S.1093
[25] F. Boudou, A. E. Sabar, M. I. Majeed, A. M. Ibraham, R. Jamal, A. Rashid, A. Belakredar, M. Bendahmane-Salmi, M. RASHEED, R. RASHEED, T. Saidani, H. D. Al-Bahadli, Experimental and Theoretical NANOTECHNOLOGY, 10 (2026) 821. https://doi.org/10.56053/10.S.821
[26] A. R. J. Katae, H. H. Hussein, A. S. Jaber, M. A. Sarhan, M. RASHEED, Experimental and Theoretical NANOTECHNOLOGY, 10 (2026) 725. https://doi.org/10.56053/10.2.725
[27] G. E. Alkinani, A. R. J. Katae, M. RASHEED, Experimental and Theoretical NANOTECHNOLOGY, 10 (2026) 1027. https://doi.org/10.56053/10.S.1027
[28] A. R. J. Katae, H. H. Hussein, A. S. Jaber, M. A. Sarhan, M. RASHEED, Experimental and Theoretical NANOTECHNOLOGY, 10 (2026) 795. https://doi.org/10.56053/10.2.795
[29] H. K. Aity, E. Dhahri, M. Rasheed, Ceramics International, 50 (2024) 54666. https://doi.org/10.1016/j.ceramint.2024.10.324
[30] T. Saidani, M. Rasheed, I. Alshalal, A. A. Rashed, M. A. Sarhan, R. Barillé, Research on Engineering Structures and Materials, 9 (2023) 1. https://doi.org/10.17515/resm2023.21ma0922rs
[31] M. Rasheed, S. Shihab, O. Alabdali, A. Rashid, T. Rashid, Journal of Physics: Conference Series, 1999 (2021) 012077. https://doi.org/10.1088/1742-6596/1999/1/012077

[32] M. Rasheed, R. Barillé, Journal of Alloys and Compounds, 728 (2017) 1186. https://doi.org/10.1016/j.jallcom.2017.09.084
[33] W. Saidi, N. Hfaidh, M. Rasheed, M. Girtan, A. Megriche, M. El Maaoui, RSC Advances, 6 (2016) 68819. https://doi.org/10.1039/c6ra15060h